Preliminary Approach to Assess the Seismic Hazard on a Lunar Site

Santiago Ruiz[a], Alejandro Cruz[a], Daniel Gomez[a,*], Shirley J. Dyke[b,c], Julio Ramirez[c]

[a]*School of Civil Engineering and Geomatics, Universidad del Valle, Cali, Colombia*
[b]*School of Mechanical Engineering, Purdue University, West Lafayette, 47907, IN, USA.*
[c]*Lyles School of Civil Engineering, Purdue University, West Lafayette, 47907, IN, USA.*

Abstract

The passive seismic network deployed on the Moon during the Apollo missions operated for eight years and allowed the observation of seismic activity. More than 12500 seismic events were registered, where 28 were classified as shallow moonquakes with moment magnitudes up to 4.1. Seismic events of this nature pose a significant risk to future long-term lunar habitats; thus, these events must be carefully studied and considered in the seismic design of these structures. This paper proposes a preliminary seismic hazard assessment imposed by shallow moonquakes. The hazard assessment is performed using the Probabilistic Seismic Hazard Analysis (PSHA) methodology, considering previous studies and theories regarding the seismic environment of the Moon. The study zone covers $\sim$ 860 km^2 of the Taurus-Littrow Valley, containing the Apollo 17 landing site and the Lee-Lincoln lobate scarp as the considered seismic source. The seismic hazard is quantified in terms of peak ground acceleration (PGA) and spectral acceleration (5% damped pseudo-acceleration, PSA). Seismic hazard deaggregation scenarios, Uniform Hazard Spectra (UHS) for different hazard levels, and a Conditional Mean Spectrum (CMS) for a target period of 0.2 s are obtained to quantify the seismic hazard on a specific site on the Moon. The developed seismic hazard assessment provides a preliminary approach for realistic scenarios to conduct structural designs that ensure the seismic performance of fully operational long-term lunar structures.

Keywords: Moonquake, Seismic hazard, Lobate scarp, Design spectra

*Corresponding author.
Email address: `daniel.gomez@correounivalle.edu.co` (Daniel Gomez)

1. Introduction

For the last few decades, different government agencies and private companies have envisioned the creation of safe extraterrestrial habitats on the Moon. The development of permanent settlements is required since its proximity to Earth represents the most significant advantage for colonization, tourism and supply operations (Benaroya, 2018; Schmelzbach et al., 2020; Theinat et al., 2020). In this extremely hostile environment, a lunar base will be exposed to several hazards which need to be identified and characterized to develop safe and resilient structural designs (Maghareh et al., 2018; Cohen and Team, 2009; Reid, 2020). One of these hazards is produced by the seismic activity on the Moon.

The Apollo Passive Seismic Experiments (APSE) consisted of four seismic stations network deployed on the lunar surface during the Apollo program missions 12, 14, 15 and 16, between 1969 and 1972 (Nunn et al., 2020). Each station was equipped with passive seismometers capable of measuring the horizontal and vertical components of the Moon's surface motion (Nunn et al., 2020). Data were collected and transmitted back to the Earth from 1969 to 1977 (Nakamura et al., 1982). The network was located on the near side of the Moon in a triangular distribution with a distance between stations of approximately 1100 km and was able to detect more than 12000 seismic events (moonquakes) (Khan and Mosegaard, 2002). These events were classified according to their type of source as deep, thermal, impacts and shallow (Nakamura et al., 1982).

Deep moonquakes are the most numerous events with more than 7000 records, and they are unlikely to represent a risk for a lunar habitat, with estimations of body wave magnitudes for the largest events of ~3.0 and depths greater than 700 km (Goins et al., 1981; Lognonné and Johnson, 2007). Recent estimations indicate moment magnitudes from 2.3 to 3.3 (Kawamura et al., 2017), repetitive waveforms and dominant frequency content (~0.5 Hz) have allowed researchers to relate their origin to tidal forces generated by the interaction of the Earth and Moon (Latham et al., 1971; Nakamura, 2005). Thermal moonquakes are the seismic events with the smallest associated amplitudes. Similar to deep moonquakes, these events are unlikely to cause damage to a lunar habitat (Mottaghi and Benaroya, 2015). They present periodic temporal and spatial occurrences with similar waveforms and amplitudes (Duennebier and Sutton, 1974). It is believed that this type of moonquake occurs as a consequence of the expansion and contraction of the lunar crust caused by temperature gradients between the lunar day and night (Duennebier and Sutton, 1974). Impact events have their origin in meteoroid impacts (comets, asteroids and interstellar debris) and artificial impacts caused by spacecrafts. The signals of these events are characterized by abrupt P-wave arrivals and the absence of S-waves (Nakamura et al., 1974). Finally, shallow moonquakes are believed to pose a significant risk to a lunar base as they have the biggest amplitudes with associated body-wave magnitudes up to 5.8 (Oberst, 1987; Oberst and Nakamura, 1992; Mottaghi and Benaroya, 2015). The few recorded events and the uncertainties in estimating the hypocenters impose difficulty in understanding the mechanisms for their generation (Nakamura, 1980). Some authors suggest that thermal influences may cause them due to surface temperature variations, intraplate tectonics or the Moon's interaction with high energy particles (Frohlich and Nakamura, 2006). Recent findings by Watters et al. (2019) suggest that shallow moonquakes are triggered by a vast globally distributed network of lobate scarps, observed on the Moon's surface by the cameras of the Lunar Reconnaissance Orbiter (LRO) spacecraft.

The existence of a significant and potentially strong lunar seismic activity, mainly caused by shallow moonquakes, emphasizes the importance of characterizing expected ground motions by performing a seismic hazard analysis. Seismic hazard analysis provides information on the probabilities of certain levels of ground motion occurring over a period of time related to the operating time of a structure (Baker, 2013). This information is used to determine design requirements for structures to withstand the predicted seismic scenarios (Kramer, 1996). It is critical to determine these requirements in future long-term lunar habitats design, since any structural failure in these extraterrestrial structures would represent an imminent threat to their occupants (Oberst and Nakamura, 1992; Benaroya, 1994).

This paper aims to perform a preliminary assessment of the seismic hazard imposed by shallow moonquakes on a lunar site using the Probabilistic Seismic Hazard Analysis (PSHA) methodology. With this probabilistic approach, the effects of all the moonquakes expected to occur on a zone during a specified time period are integrated, involving the associated epistemic and aleatory uncertainties. This work includes selecting a study site, identifying and describing a seismic source, characterizing the event occurrence and selecting Ground Motion Prediction Equations (GMPEs). The obtained results in this study provide a preliminary understanding of the seismic hazard environment of the Moon through hazard curves and seismic hazard extensions that include deaggregation of events, Uniform Hazard Spectra (UHS) and Conditional Mean Spectra (CMS).

The organization of this paper is as follows. In Section 2, the methodology and general considerations of the PSHA are described. This section depicts all the steps performed in the PSHA based on the shallow events on the Moon. The results are shown and analyzed in Section 3, where different hazard spectra are proposed. Finally, the main findings, recommendations and potential applications for these results are presented in the Conclusions.

2. Methodology

The PSHA methodology has become the most widely used approach to determine the expected ground motion characteristics of a seismically active site (Bommer, 2002). The PSHA is implemented in this study to assess the seismic hazard imposed by shallow moonquakes. This methodology aims to quantify the aleatory and epistemic uncertainties involved in the seismic hazard analysis, recognizing that certain essential aspects of the origin and behavior of quakes are unknown (Baker, 2013). Aleatory uncertainties are incorporated in this analysis, considering seismic events with all possible combinations of magnitudes and distances. Epistemic uncertainties, related to the lack of knowledge of the value of a variable or a model (Sianko et al., 2020), are incorporated into this work using the logic tree configuration.

The process to perform the PSHA consists of the following five steps: *a*) definition of the seismic catalog; *b*) selection of the study site and identification of seismic sources; *c*) calculation of the seismic parameters; *d*) selection of GMPEs; and *e*) seismic hazard calculation. By calculating the seismic hazard, plots of the annual frequency of exceedance vs. peak ground acceleration or spectral acceleration are obtained as hazard curves. These results are then used to perform the seismic hazard deaggregation, calculating the UHS and CMS for different hazard levels.

The seismic hazard is computed as

$$\lambda(\mathrm{IM} > x) = \lambda_{min} \sum_{j=1}^{n_M} \sum_{k=1}^{n_R} P(\mathrm{IM} > x|m_j r_k) P(M = m_j) P(R = r_k) \tag{1}$$

where IM is the ground motion intensity measure parameter, $\lambda(\mathrm{IM} > x)$ is the annual rate of occurrence of $\mathrm{IM} > x$ and λ_{min} is the rate of moonquakes greater than M_c. M_c is the magnitude of completeness (Section 2.3). The terms $P(\mathrm{IM} > x|m_j r_k)$, $P(M = m_j)$ and $P(R = r_k)$ are the probability distributions of IM, moment magnitude of the event m and the source-to-site distance r, respectively. These distributions will be defined in Sections 2.2, 2.3 and 2.4. The limits of the sums (n_M and n_R) are determined according to m and r ranges (*i.e.,* M_c and M_{max}, r_{min} and r_{max}). A MATLAB algorithm developed for this study was implemented to calculate the seismic hazard. This computer routine was validated with a benchmark PSHA example from Kramer (1996).

2.1. Seismic catalog: Shallow moonquakes

The seismic hazard on a lunar site is calculated considering only shallow moonquakes, as these are the most likely to cause damage to a lunar base due to their considerable stress drops of up to 100 MPa and body-wave magnitudes up to 5.8 (Oberst, 1987; Oberst and Nakamura, 1992; Watters et al., 2019). By contrast, this analysis does not consider thermal and deep moonquakes because their low magnitudes and energy released do not represent significant safety implications for future lunar settlements. Vibrations due to meteorite impacts, despite being generated on the surface and having similar ground motion amplitudes to shallow moonquakes, are excluded from this analysis because their external origins do not represent the seismicity of the Moon's internal structure, requiring a different hazard approach (Oberst and Nakamura, 1992).

This hazard assessment considers the 28 shallow moonquakes shown in Table 1, which corresponds to the identified events of this type during the eight years of the APSE recorded data. Shallow moonquakes are the rarest in occurrence, with an average of four events detected annually (Nakamura, 1980; Nakamura et al., 1979). They are also characterized by high-frequency content and relatively well-defined arrival time of the P and S waves (Nakamura et al., 1974). To avoid magnitude saturation and maintaining the compatibility with the majority of the available GMPEs in the literature, the magnitudes of the shallow events are homogenized to the moment magnitude scale M_w proposed by Hanks and Kanamori (1979), which is given by

$$M_w = (2/3)(\log(M_o) - 9.05) \quad (2)$$

where M_o is the seismic moment (in N-m) estimated by Oberst (1987). The resulting M_w magnitudes for each event are shown in Table 1.

Table 1. Catalog of shallow moonquakes considered in this study. Seismic moment M_o values are taken from Oberst (1987), and latitude and longitude values are taken from Nakamura et al. (1979).

Year	Day	Latitude (°)	Longitude (°)	Seismic Moment M_o (Nm)	Magnitude Mw
1971	107	48	35	4.4E+14	3.7
	140	42	-24	6.6E+13	3.2
	192	43	-47	5.2E+13	3.1
1972	2	54	101	2.3E+14	3.5
	261	12	46	1.1E+13	2.7
	341	51	45	1.9E+13	2.8
	344	-20	-80	1.2E+13	2.7
1973	39	33	35	5.5E+12	2.5
	72	-84	-134	6.6E+14	3.8
	171	-1	-71	1.3E+14	3.4
	274	-37	-29	3.4E+13	3.0
1974	54	36	-16	4.7E+12	2.4
	86	-48	-106	1.5E+13	2.8
(*)	109	-37	42	1E+13	2.6
(**)	149	_	_	6.3E+13	3.2
	192	21	88	2.5E+14	3.6
1975	3	29	98	1.6E+15	4.1
	12	75	40	1.1E+14	3.3
	13	-2	-51	1E+13	2.6
	44	-19	-26	1.9E+13	2.8
	127	-49	-45	2.9E+13	2.9
	147	3	-58	2.3E+13	2.9
	314	-8	64	4.8E+13	3.1
1976	4	50	30	4.2E+13	3.0
	12	38	44	1.1E+14	3.3
	66	50	-20	3E+14	3.6
	68	-19	-12	5.6E+13	3.1
	137	77	-10	1.3E+13	2.7

(*) This event was relocated by Watters et al. (2019), and it is found to be near (~13 km) the Lee Lincoln scarp with latitude and longitude coordinates 20.09° and 30.99°, respectively.
(**) 30° from Station 16 on the east side (Nakamura et al., 1979).

2.2. *Site selection and seismic source definition*

Candidate sites for future lunar exploration include the South Pole, where there are zones with access to sunlight 86% of the year, and permanently shadowed regions containing water ice, which can be used as a resource to ensure long-term exploration activities (Bussey et al., 2010; Dunbar, 2019; NASA, 2020). However, this site is not a convenient selection for this study because its geology and seismicity are still unknown (Schmelzbach et al., 2020). Another area of interest is the Taurus Littrow Valley, which contains the Apollo 17 landing site and was partially explored by astronauts Eugene Cernan and Harrison Schmitt. The performed field and sample studies provided valuable preliminary geologic information, making this valley a primary target for future scientific exploration (Taylor, 1992; Burke, 2018). Moreover, shallow seismic activity was recorded in this area according to Watters et al. (2019); therefore, it was decided to select part of this valley as the study zone based on its seismic record.

The area of the study zone is approximately 860 km^2 and is delimited by latitudes $20 - 21°$ and longitudes $30 - 31°$ (Fig. 1A). This region is crossed by the Lee-Lincoln lobate scarp (Fig. 1B), which is the fault considered the seismic source in this study. Recent evidence suggests that the Lee-Lincoln scarp is likely to be seismically active. The evidence includes regolith disturbance and boulder movements in nearby areas (Watters et al., 2019). Lobate scarps of faults are interpreted as manifestations of low-angle thrust faults (Hargitai and Kereszturi, 2015), having scarp faces with slopes between $\sim 5°$ to $29°$ and an estimated age of less than 1 billion years (Banks et al., 2012; Williams et al., 2013).

The Lee-Lincoln scarp (20.27° N, 30.56° E) has a length of ~14 km and is located ~13 km from a relocated moonquake epicenter by Watters et al. (2019) (Table 1). The fault dip angle θ is taken as $30°$ and the depth is assumed to be 1 km, based on the estimations made by Banks et al. (2012). The seismic potential of the Lee-Lincoln is estimated with the relationship of Wells and Coppersmith (1994) given by

$$M_w^{(LL)} = 5.08 + 1.16 \cdot \log(\text{SRL}) \tag{3}$$

where SRL is the Source Rupture Length of the observed trace fault. This model was developed with empirical data from faults on Earth and due to the absence in the literature of a similar relationship between lobate scarps and moment magnitudes, this paper assumes that the model of Wells and Coppersmith (1994) is applicable in the lunar context. The use of this relation for lobate scarps has also been suggested by Kumar et al. (2016). By replacing SRL with 14 km in Eq. (3), a maximum moment magnitude for the Lee-Lincoln scarp of $M_w^{LL} = 6.4$ is obtained. Therefore, the hazard calculation is performed taking this value as the magnitude's upper limit $M_{max} = M_w^{LL}$.

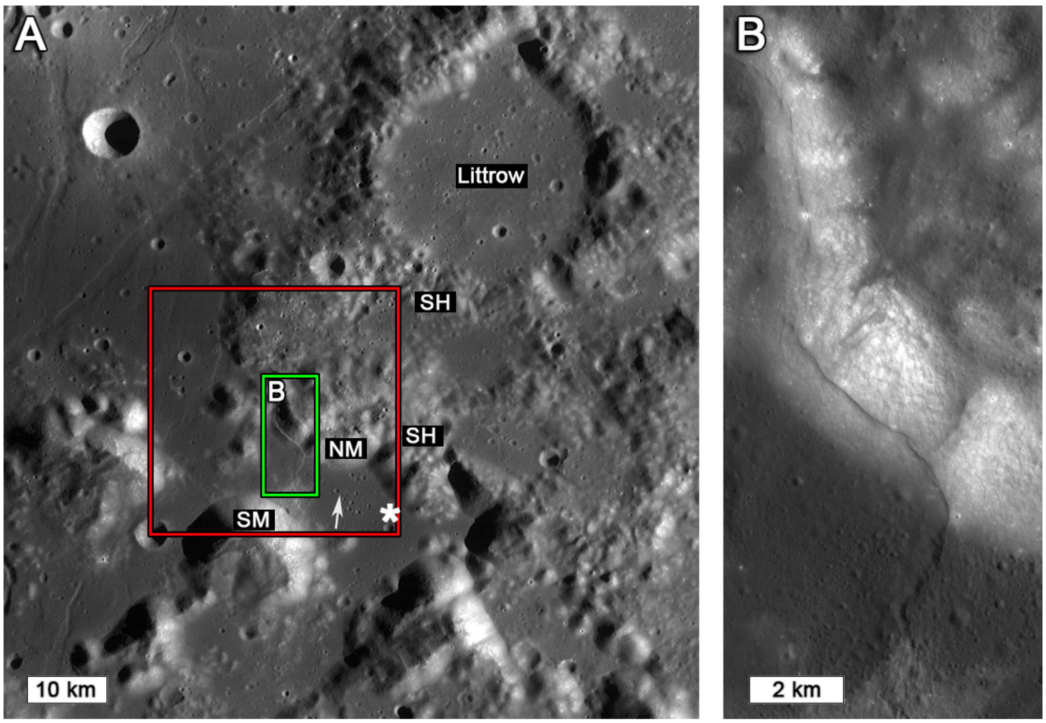

Fig. 1. Lunar Reconnaissance Orbiter Wide Angle Camera (LROC WAC). A.) Mosaic is looking down at the Taurus-Littrow Valley area. The area enclosed by the red box is the selected study zone ($\sim$ 860 km^2). SM = South Massiff, NM = North Massif, SH = Sculptured Hills. The arrow indicates the Apollo 17 landing site, and the asterisk shows the epicenter of the moonquake relocated by Watters et al. (2019). North is up. [NASA/GSFC/Arizona State University]. B.) Lee-Lincoln scarp in the Taurus-Littrow Valley (LROC NAC image frame M104318871LE) [NASA/GSFC/Arizona State University].

The seismic source (Lee-Lincoln Scarp) is modeled as a linear fault. In the PSHA methodology, seismic events are considered equally likely to occur anywhere on the fault (Kramer, 1996). With this assumption, one can then describe the spatial uncertainty of the source by employing a source-to-site distance (r) probability distribution. In this study, the distance parameter is taken as the epicentral distance and the probability distribution is constructed using a histogram. The process consisted of selecting 10 distance bins and then dividing the source into 100 equal segments to make a more accurate calculation of the distribution. Lastly, the epicentral distance from the site to the midpoint of each fault segment is measured and assigned to the corresponding bin in which it is located.

Fig. 2 shows the probability distribution of the epicentral distance *P(R=r)* to a point corresponding to the Apollo 17 landing site, which is taken as a reference. It is noted that the probabilities associated with the 10 distance bins considered in the calculation sum up to 1. The probability is 0 when distances outside of the range (Fig. 2) are evaluated because the lower and upper limits of this range represent the minimum r_{min} and maximum r_{max} epicentral distances from the site to the seismic source. For this case, the evaluated distances are in the range of 5.8 to 15.6 km.

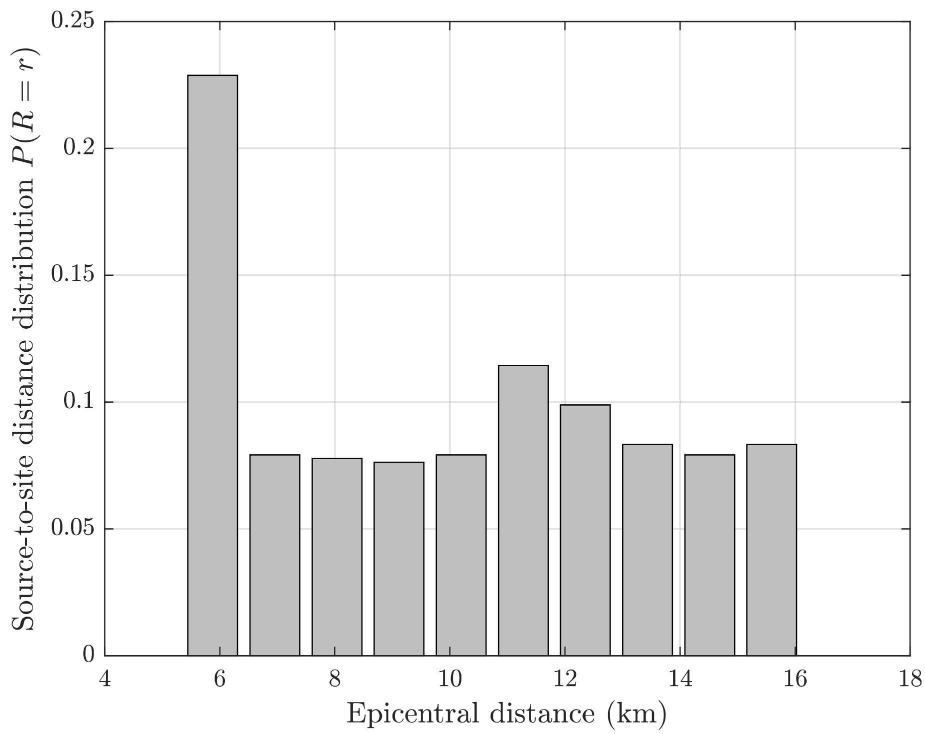

Fig. 2. Source-to-site probability distribution of the Lee-Lincoln fault scarp. Apollo 17 landing site coordinates: 20.19° N, 30.77 °E.

2.3. Calculation of seismicity parameters

The seismicity parameters are used to describe the relationship between the frequency of occurrence of moonquakes and their magnitudes. This relationship is incorporated into the calculation of the seismic hazard using a probability density function (PDF) of the magnitude distribution (Eq. (6)), obtained from the doubly truncated Gutenberg–Richter Recurrence Law (GR Law) (Gutenberg and Richter, 1944) of Eq. (4)

$$N(m \geq M) = N_{M_c} \cdot \exp(-\beta(m - M_c)) \tag{4}$$

where N is the cumulative number of events with a magnitude m equal to or greater than the evaluated magnitude M (M_w), β is defined as $\beta = b \cdot \ln(10)$, where b (b value) is a coefficient that represents the proportion of small magnitude events to those of large magnitudes, N_{M_c} is the cumulative number of events with moment magnitude greater than the minimum magnitude of completeness M_c (Kramer, 1996). M_c is estimated using the method proposed by Wiemer and Wyss (2000). The method consists of first, calculating the seismicity parameters of the GR Law (i.e., a and b values) with the use of a maximum likelihood estimation (Eq. (8)) based on events with magnitude equal to or greater than M_i, for i covering the entire magnitude range of the seismic catalog of Table 1. Next, a synthetic distribution of magnitudes (GR Law) is computed for every set of a, b and M_i values. Then, the goodness-of-fit (R) between the observed cumulative number of events (B_i) and the predicted values (S_i) is calculated as

$$R\,(a, b, M_i) = 100\; - \left(\frac{\sum_{M_i}^{M_{max}} B_i - S_i}{\sum_i B_i} \right). \tag{5}$$

In this study, the value of M_c corresponds to the one that generates a goodness-of-fit value R of 90%. The obtained M_c was 3.1; thus, when the M_c is 3.1, the synthetic distribution can describe 90% or more of the frequency-magnitude distribution. M_{max} is the maximum magnitude defined in Section 2.2.

The PDF of the magnitude distribution of Eq. (4) is defined as

$$f_M(m) = \beta \frac{\exp(-\beta(m - M_c)}{1 - \exp(-\beta(M_{max} - M_c))}. \tag{6}$$

This PDF considers a continuous random value of m. However, for computational purposes, it is convenient to treat m as a discrete variable; thus, Eq. (6) is incorporated in the calculation of the seismic hazard (Eq. (1)) as

$$P(M = m) = F_M(m + \Delta M) - F_M(m) \tag{7}$$

where F_M is obtained by integrating $f_M(m)$ (Baker, 2013) and ΔM is the magnitude bin taken as 0.1.

The b value is estimated using the maximum likelihood (MLE) method (Aki, 1965), with b defined as

$$b = \frac{\log_{10}(\exp)}{\bar{M} - (M_c - \frac{\Delta M}{2})} \tag{8}$$

where $\bar{M}$ is the mean magnitude of the events in the range of $M_c \leq m \leq M_{max}$. The standard error of b is estimated from Shi and Bolt (1982) as

$$\sigma_b = 2.30 \cdot b^2 \cdot \sqrt{\frac{\sum_{i=1}^{N_e} (M_i - \hat{\mu})^2}{N_e(N_e - 1)}} \tag{9}$$

where N_e is the number of events and $\hat{\mu}$ is the sampling average of the magnitudes.

To take this uncertainty into the seismic hazard model, the resulting values of b and $b \pm \sigma_b$ are used to define three different branches of the logic tree of this study (Fig. 6), assigning a lower weight to $b \pm \sigma_b$. The resulting values and weights are shown in Table 2.

Table 2. Values of parameter b and assigned weights for logic tree branches.

	$b = 1.04$	$b + \sigma_b = 1.25$	$b - \sigma_b = 0.83$
Assigned weight	0.7	0.15	0.15

Using the three calculated values for b in Ec. (7), the probability distributions in Fig. 3 are obtained.

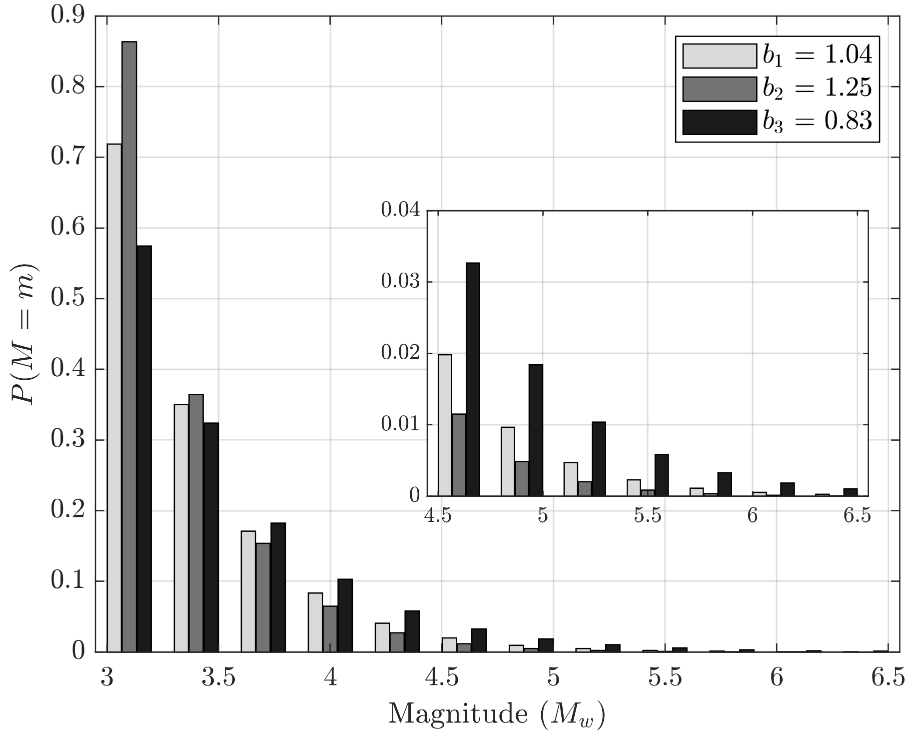

Fig. 3. Magnitude probability distribution of shallow moonquakes.

2.4. *Selection of ground motion prediction equations*

GMPEs allow the evaluation of the effects that events with all possible combinations of m and r have in the study zone (Gupta, 2002). These effects are expressed in terms of the predicted mean value of a selected IM. The selected IM parameters for this study are the peak ground acceleration (PGA) and the spectral acceleration (5% damped pseudo-acceleration, PSA) at spectral periods T up to 3 s for horizontal components of shaking. These parameters can describe the amplitude of the ground motion and are widely used in seismic engineering and structural response analysis. The predicted IM serves as input to Eq. (1) for the computation of seismic hazard as

$$P(\mathrm{IM} > x \mid m, r) = 1 - \Phi\left(\frac{\ln x - \overline{\ln \mathrm{IM}}}{\sigma_{\ln \mathrm{IM}}}\right) \tag{10}$$

where $P(\mathrm{IM} > x \mid m, r)$ is the probability that IM exceeds a certain value x for a given m and r, Φ is the standard normal cumulative distribution function, $\ln x$ is the natural logarithm of the evaluated value x, $\ln \mathrm{IM}$ is the natural logarithm of the mean predicted IM parameter and $\sigma_{\ln \mathrm{IM}}$ is the standard deviation of $\ln \mathrm{IM}$.

The recorded shallow moonquakes do not provide sufficient events to develop a GMPE based on experimental data. Thus, at least two options to address the lack of the seismic information are available in the literature: a.) developing a model from synthetic accelerograms (Schleicher et al., 2020), or b.) using traditional GMPEs that meet specific applicability criteria. The first option is beyond the scope of this work; therefore, the traditional GMPEs models shown in Table 3 are selected and included in the analysis.

Table 3. List and abbreviations of the selected GMPEs.

Reference to GMPE	Abbreviation
Bommer et al. (2007)	BO-07
Akkar and Bommer (2010)	AKK-10
Atkinson and Boore (2011)	AB-11
Zalachoris and Rathje (2019)	ZR-19
Abrahamson et al. (2014)	ASK-14

The selection criteria for the GMPEs include their applicability in the established ranges of m, r and T. Furthermore, considering that basaltic layers underlie the Taurus-Littrow Valley (Sollberger et al., 2016; Schmitt et al., 2017), GMPEs that have been applied in areas with basaltic soil in previous Earth seismic hazard studies were selected. The scope of this work is limited to selecting models available in the literature that are considered appropriate for this case study, recognizing that future refinements of the hazard model will require the development of proper GMPEs for the Moon.

The ASK-14 model can be used for all ranges of m and T considered in the analysis; thus, this model is assigned to an individual branch of the logic tree (Fig. 6). On the other hand, the BO-07, AKK-10, AB-11 and ZR-19 models are only valid for certain ranges of m and T. A model is needed that covers the full range of these parameters. Therefore, the four models are merged into one model denominated G3-Model, so that the final response satisfies the entire proposed m and T ranges.

The model's integration in the G3-Model consisted of assigning weights to each GMPE according to their applicability ranges, following the same concept of a logic tree configuration (the models are mutually exclusive and collectively exhaustive). When more than one model is available for an applicability range, it is decided to assign equal weights to each one, considering that it is not certain how well the respective model describes the actual propagation of the seismic waves in the corresponding ranges. The adopted weights and applicability ranges for the construction of the G3-Model are shown in Table 4. Additionally, Appendix A presents the equations of all GMPEs used in this work, with the definition of their parameters and applicability ranges.

Table 4. Magnitude and spectral period ranges for the G3-Model assemble. The assigned weights are shown in parentheses.

Magnitude M_w	Spectral period T (s)		
	0-0.05	0.05-0.5	0.5-3
3-3.5	ZR-19 (1)	BO-07 (0.5) ZR-19 (0.5)	ZR-19 (1)
3.5-5.5	ZR-19 (0.5) AB-11 (0.5)	BO-07 (1/3) ZR-19 (1/3) AB-11 (1/3)	ZR-19 (0.5) AB-11 (0.5)
>5.5	AKK-10 (0.5) AB-11 (0.5)	BO-07 (1/3) AKK-10 (1/3) AB-11 (1/3)	AKK-10 (0.5) AB-11 (0.5)

The final weights assigned to the G3-Model and ASK-14 models in the logic tree of the analysis (Fig. 6) are calculated following the methodology proposed by Wang and Lin (2021). It allows the definition of the weights assigned to different logic tree attenuation models as probabilities, instead of subjective values of each model's degree of certainty or degree of belief. This new methodology follows a Bayesian approach and is expressed as

$$\mathrm{Pr}''\left(\eta_i\right) = \frac{\mathrm{Pr}'\left(\eta_i\right) \times \mathrm{Pr}\left(\alpha \mid \eta_i\right)}{\sum_{i=1}^{n} \mathrm{Pr}'\left(\eta_i\right) \times \mathrm{Pr}\left(\alpha \mid \eta_i\right)} \tag{11}$$

where η is the natural logarithm of PGA predicted from the probability distribution of the i-th GMPE, α is the actual PGA observation of the site of interest, $\mathrm{Pr}'\left(\eta_i\right)$ denotes the preassigned probability to the i-th model and $\mathrm{Pr}''\left(\eta_i\right)$ is its posterior probability updated with the observed PGA. The term $\mathrm{Pr}\left(\alpha \mid \eta_i\right)$ is the probability that the observed PGA (i.e., α) will occur given the η_i prediction of the i-th model.

Because the observed PGA values of the moonquakes were obtained for distances greater than those of applicability of the GMPEs (>500 km), in this work is decided to use synthetic observed values of PGA, calculated by Mohanty et al. (2020), which are generated for ranges of 0-50 km and 0-100 km. For the calculation of model weights with Eq. (11), four observed (synthetic α) values were considered, which correspond to the PGA of a magnitude 4.0 (M_w) moonquake with epicentral distances of 5, 10, 20, and 30 km, respectively. Fig. 4 shows the PGA as a function of epicentral distance for the synthetic model and the two selected attenuation models.

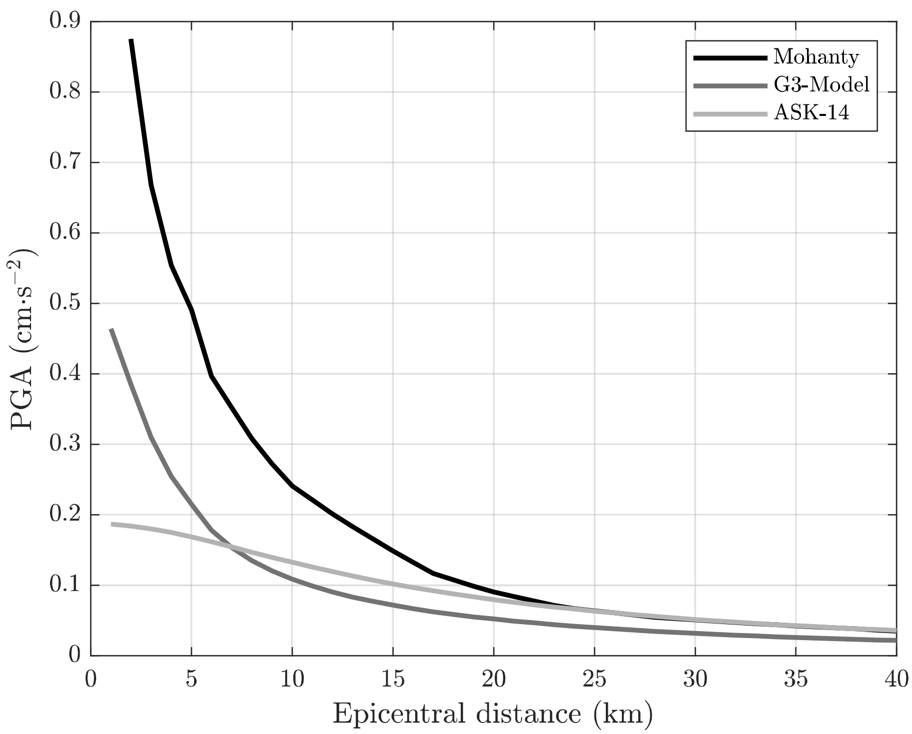

Fig. 4. Variation of PGA of 4.0 (M_w) moonquake with epicentral distances of the selected GMPEs and synthetic values from Mohanty et al. (2020).

Without any substantial evidence to support the applicability of the models ASK-14 and G3-Model, the probability $\Pr'(\eta_i)$ for each model is considered to be 0.5 before the Bayesian updating. The probabilities $\Pr(\alpha \mid \eta_i)$ obtained for the G3-Model and ASK-14 models were 0.0150 and 0.0068, respectively. Therefore, the respective updated probabilities ($\Pr''(\eta_i)$) of both models are 0.6883 and 0.3117, which are assigned as the weights to the logic tree branches of the analysis (Fig. 6).

The response spectra for a M_w=4 event with an epicentral distance of 10 km for both the ASK-14 and G3-Model are shown in Fig. 5 for illustrative purposes. Note that the response of the G3-Model is less smooth than the output of ASK-14 due to the incorporation of the different models in its construction.

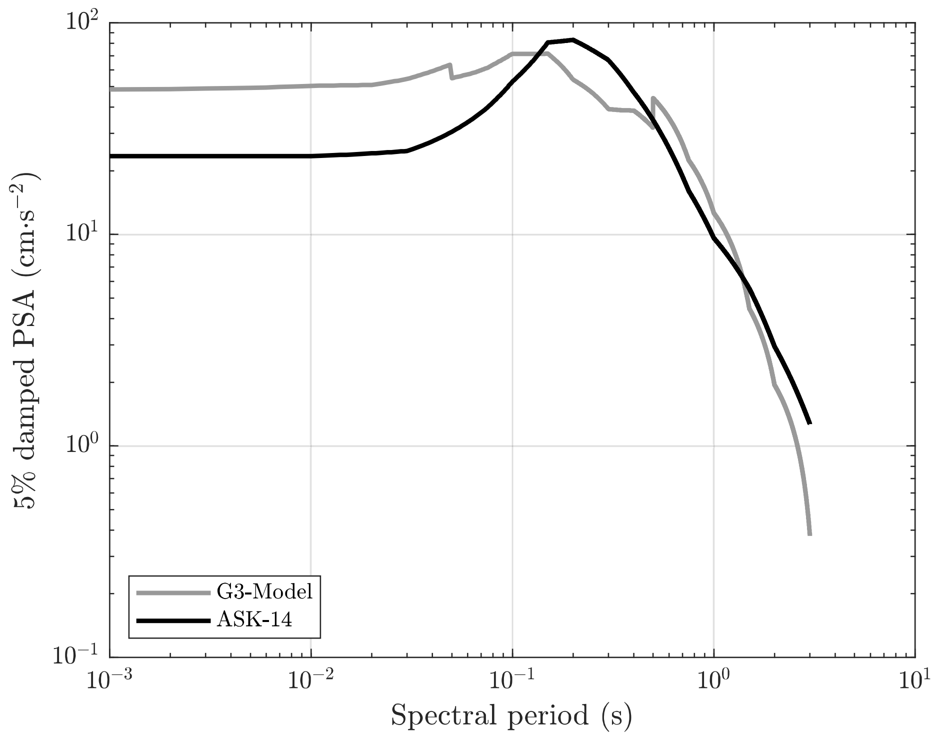

Fig. 5. Response spectra for a M_w=4 moonquake at an epicentral distance of 10 km.

In addition to the magnitude and distance, GMPEs require input parameters that describe the site conditions and fault mechanisms. The seismic source parameters are taken based on the characterization of the Lee-Lincoln scarp in Section 2.2. Moreover, the correction of the source-to-site distances is performed according to the required input of each GMPE. The average shear-wave velocity at 30 m below the surface is taken as 90 m·s^{-1}, estimated from the seismic velocity model developed by Sollberger et al. (2016).

2.5. Seismic hazard calculation

The seismic hazard is computed using Eq. (1) for an established x range, and it is performed for each branch path of the logic tree (Fig. 6). Since three b values and two GMPEs are included in the logic tree, the result for a single IM consists of six hazard curves that are combined into a single output by performing a weighted average. The assigned weights for each b value and GMPE model obtained in Section 2.3 are shown below their value and model name. The final weights of each hazard curve before the combination are calculated by multiplying all the established weights along with the components of the branches (Bommer et al., 2005). From the resulting hazard curves, it is possible to read the level of ground motion for a given annual rate of occurrence. They are also used to construct the UHS, CMS and the calculation of the seismic deaggregation (Baker, 2013, 2011).

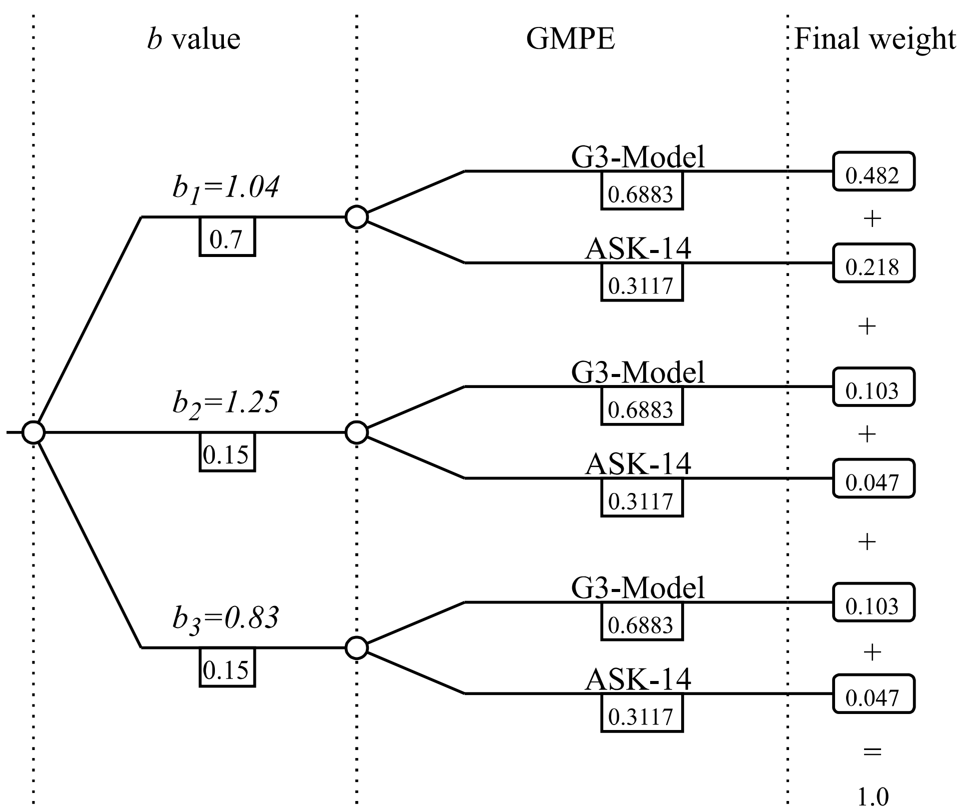

Fig. 6. The formulated logic tree used in the PSHA.

3. Results

3.1. Seismic hazard curves and PGA variation

The Apollo 17 landing site ($20.19° N, 30.76° E$) is taken as a reference site to perform the seismic hazard calculations. The hazard curves obtained for this site are shown in Fig. 7. A deterministic value of PGA associated with a specific return period T_r, which inverse value is the annual rate of occurrence λ, is used to describe the seismic hazard level at a specific site. The T_r is a time interval of an event for which the probability of occurrence is uniformly distributed in that period. Because there is no confidence in the occurrence of seismic events in terms of the T_r, the probability of exceedance p of a ground motion in n years is incorporated into the PSHA analysis. The T_r is calculated with Eq. (12) as

$$T_r = \frac{1}{1 - (1 - p)^{\frac{1}{n}}}. \tag{12}$$

Long-term habitat design should meet specific performance objectives for different hazard levels in the structural design. The structural response to different seismic demands will determine the appropriate return periods for the design, considering that lunar structures will have different design requirements than those on Earth. In this study, to demonstrate the use of the return period in the PSHA methodology, a probability of exceedance of 10% in 50 years is selected. By replacing these two values in Eq. (12), a T_r of 475 years is obtained. The PGA associated with this hazard level is obtained by reading the acceleration corresponding to the annual rate of occurrence λ=1/T_r from Fig. 7.

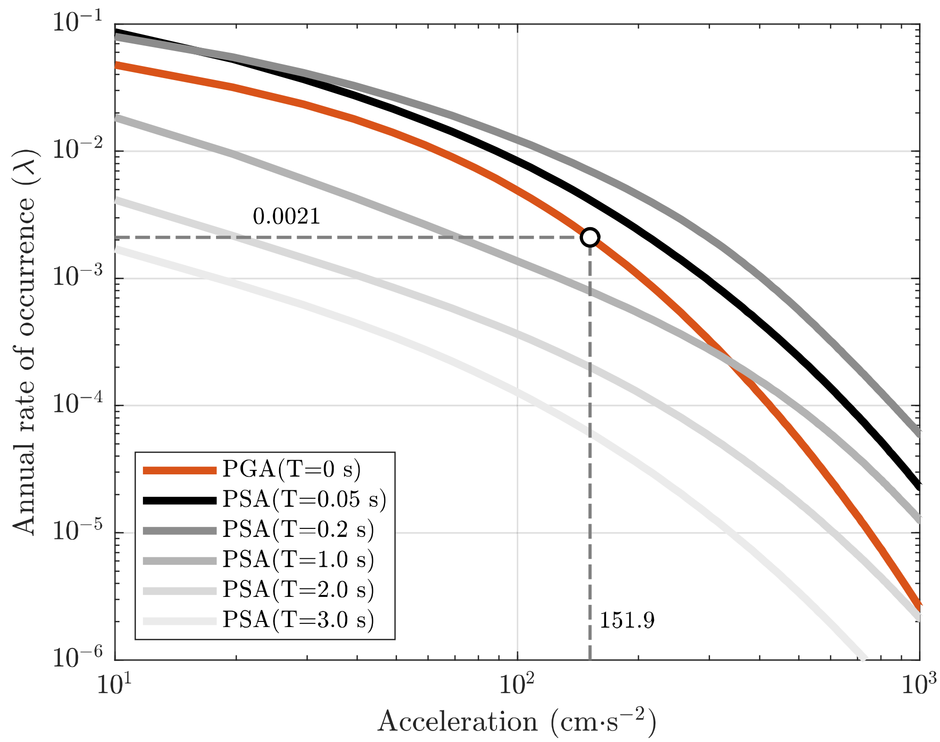

Fig. 7. Seismic hazard curves for PGA and PSA at different periods. The marked point corresponds to the deterministic value of PGA with T_r=475 years (λ=0.0021).

To explore the PGA variation with a T_r of 475 years in the study zone, the seismic hazard calculation described in Section 2.5 is performed every 0.25°. The results are interpolated to obtain the PGA at intermediate points, as shown in the seismic hazard map (Fig. 8). From this map, it can be seen how the PGA varies as a function of the epicentral distance. Three contour lines corresponding to ground accelerations of 100, 170 and 250 cm·s^{-2} are highlighted to observe the PGA variation. The maximum acceleration obtained at the center of the fault is approximately 280 cm·s^{-2}.

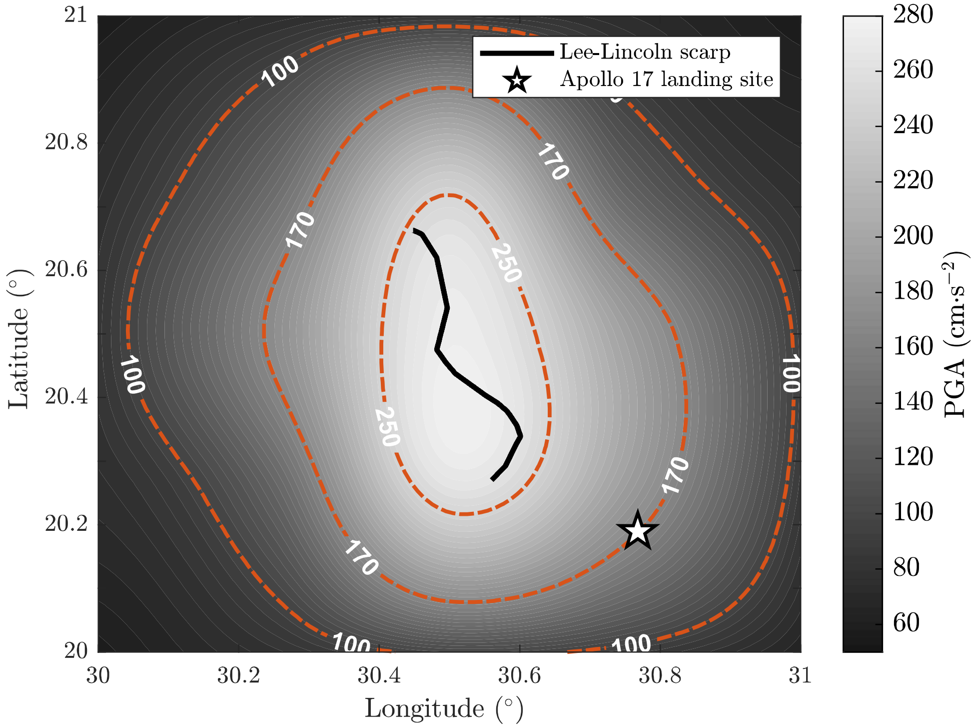

Fig. 8. Seismic hazard map of the study zone in terms of PGA with T_r= 475 years. 1° is approximately 30.32 km.

3.2. Seismic hazard deaggregation

The seismic hazard curves (Fig. 7) showed the expected accelerations for the effect of all possible combinations of seismic event magnitudes and epicentral distances. However, it is of interest to know which events are likely to cause a certain level of hazard that are not possible to observe directly from the hazard curves (Gupta, 2002). Hence, the deaggregation of the seismic hazard as a function of the magnitude and distance is carried out. To calculate the relative contribution of these pairs, Eq. (1) is solved for a hazard level determined by a specific annual rate of occurrence as a function of the magnitude and distance of interest (Baker, 2013). This value is then divided by the total hazard to obtain the percentage contribution of m and r, as

$$P(M = m, R = r|\text{IM} > x) = \frac{\lambda(\text{IM} > x, M = m, R = r)}{\lambda(\text{IM} > x)}. \tag{13}$$

Fig. 9 is obtained by calculating Eq. (13) for all possible combinations of m and r for a hazard level with PGA with $T_r = 475$ years. The mean values of m, r and ε obtained from the deaggregation of Fig. 9 are 4.68 M_w, 7.8 km and 5.5, respectively. ε measures the difference between the PGA associated with the deaggregation and the mean value predicted by the GMPEs ($\mu_{\ln \mathrm{PSA}}(M, R, T)$). For a given magnitude ($M = m$) and distance ($R = r$), ε is calculated as

$$\varepsilon(T) = \frac{\ln \mathrm{PSA}(T) - \mu_{\ln \mathrm{PSA}}(M, R, T)}{\sigma_{\mu_{\ln \mathrm{PSA}(T)}}}. \tag{14}$$

where $\sigma_{\ln PSA(T)}$ is the standard deviation of $\mu_{\ln \mathrm{PSA}(T)}$. If the spectral period T is 0 s, then $\ln \mathrm{PSA}(0\ s) =$ PGA.

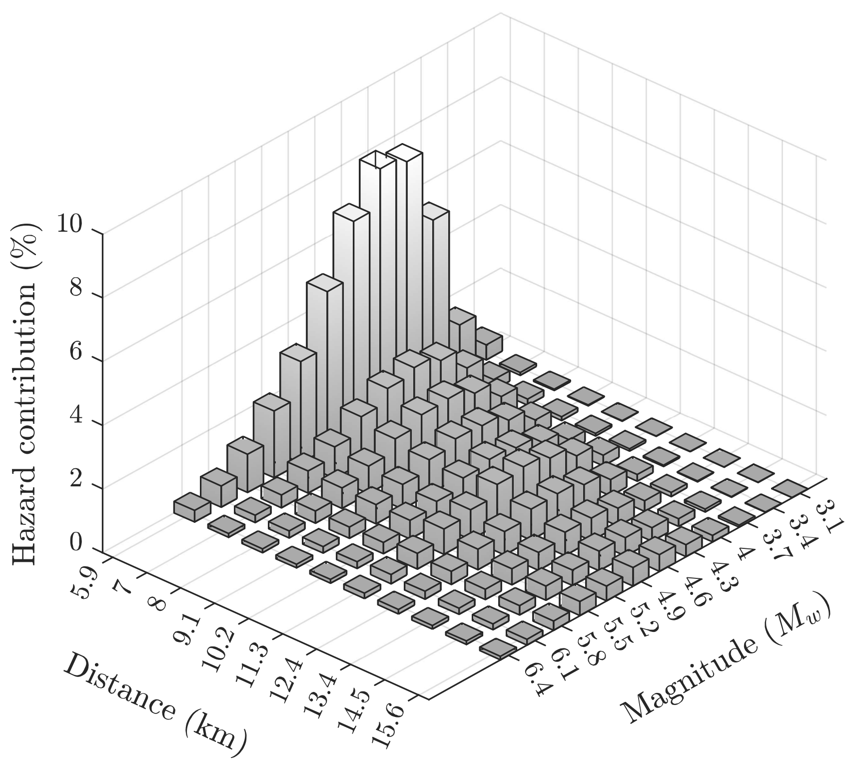

Fig. 9. Seismic hazard deaggregation for PGA with $T_r = 475$ years (Ground acceleration ≥ 151.9 cm·s^{-2}). Study site: Apollo 17 landing site.

The events that contribute the most to the seismic hazard at the reference site (10.7% of contribution) have magnitudes between 4.15 and 4.45 M_w and epicentral distances from 5.3 to 6.4 km. Thus, a design moonquake to analyze the seismic response at this site using the evaluated hazard level should comply with the mentioned m and r characteristics. Additionally, the deaggregation of Fig. 10 is performed for a spectral acceleration (Sa) at $T = 0.2$ s with T_r= 475 years. The results are used in the construction of the CMS for further calculations. The evaluated spectral period T corresponds to the natural vibration period of a hypothetical lunar structure modeled as a dynamic single-degree-of freedom (SDOF) system. The mean values of m, r and ε obtained from the deaggregation of Fig. 10 are 4.63 M_w, 8.40 km and 6.9, respectively.

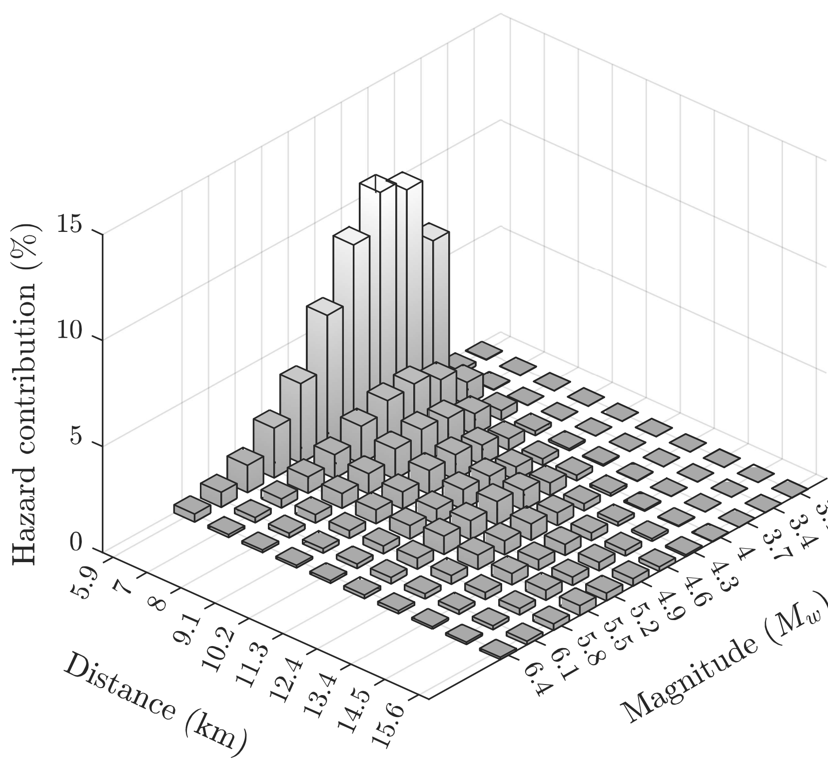

Fig. 10. Seismic hazard deaggregation for 0.2 s Sa with T_r = 475 years (Ground Acceleration $\geq$ 297.9 cm·s^{-2}). Study site: Apollo 17 landing site.

3.3. Uniform hazard spectrum (UHS)

A UHS is a spectrum whose abscissas have the same probability of being exceeded. The procedure to build this spectrum consists of choosing an annual target rate of occurrence. Then, for each hazard curve, the acceleration amplitude corresponding to that rate is picked (Baker, 2013). Fig. 11 shows the obtained UHSs for the occurrence rates of 0.0021, 0.0004 and 0.0002. These values correspond to return periods of 475, 2500, and 5000 years, respectively. Depending on the established performance requirements, one can select the appropriate spectrum for a specific structural analysis. Also, ground motions that match a UHS in Fig. 11 can be selected or scaled to be used as inputs for dynamic analysis of a lunar structure.

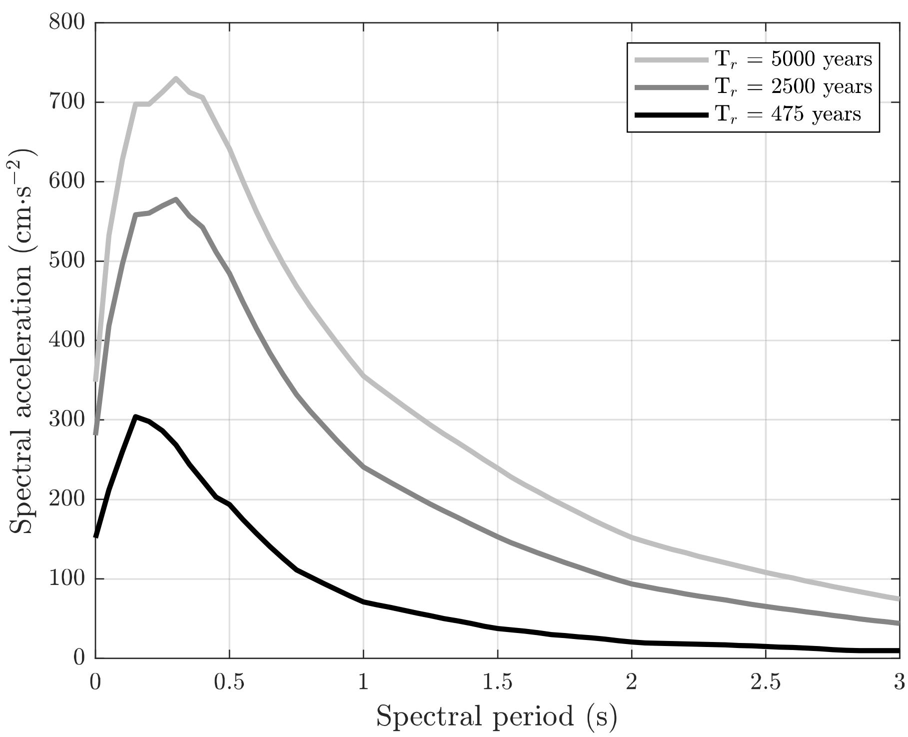

Fig. 11. Uniform hazard spectra for different T_r at the referenced site.

3.4. Conditional Mean Spectrum (CMS)

The CMS can be used as an alternative to the UHS. The response of the CMS is conditioned on the occurrence of a target spectral acceleration value $\mathrm{Sa}(T^*)$ at a specific period of interest T^* (Baker, 2011). This period is usually taken as the fundamental vibration period of a structure assumed as an SDOF system. The construction of the CMS uses the results of deaggregation for a specific $\mathrm{Sa}(T^*)$ when it is computed for a range of periods T_i, using Eq. (15)

$$\mu_{\ln \mathrm{Sa}(T_i)|\ln \mathrm{Sa}(T^*)} = \mu_{\ln \mathrm{Sa}}\left(\bar{M}, \bar{R}, T_i\right) + \rho\left(T_i, T^*\right) \varepsilon\left(T^*\right) \sigma_{\ln \mathrm{Sa}}\left(T_i\right) \tag{15}$$

where $\bar{M}$ and $\bar{R}$ are the m and r mean values obtained from the deaggregation results of a target T^* and T_r. The terms $\mu_{\ln \mathrm{Sa}}\left(\bar{M}, \bar{R}, T_i\right)$ and $\sigma_{\ln \mathrm{Sa}}\left(T_i\right)$ are the mean values and standard deviation of the natural logarithm of Sa evaluated in T_i, respectively, and $\rho\left(T_i, T^*\right)$ is a correlation coefficient (Baker, 2011). The CMS in Fig. 12 are computed for the $\bar{M}$, $\bar{R}$ and ε values obtained from the seismic hazard deaggregation in Fig. 10.

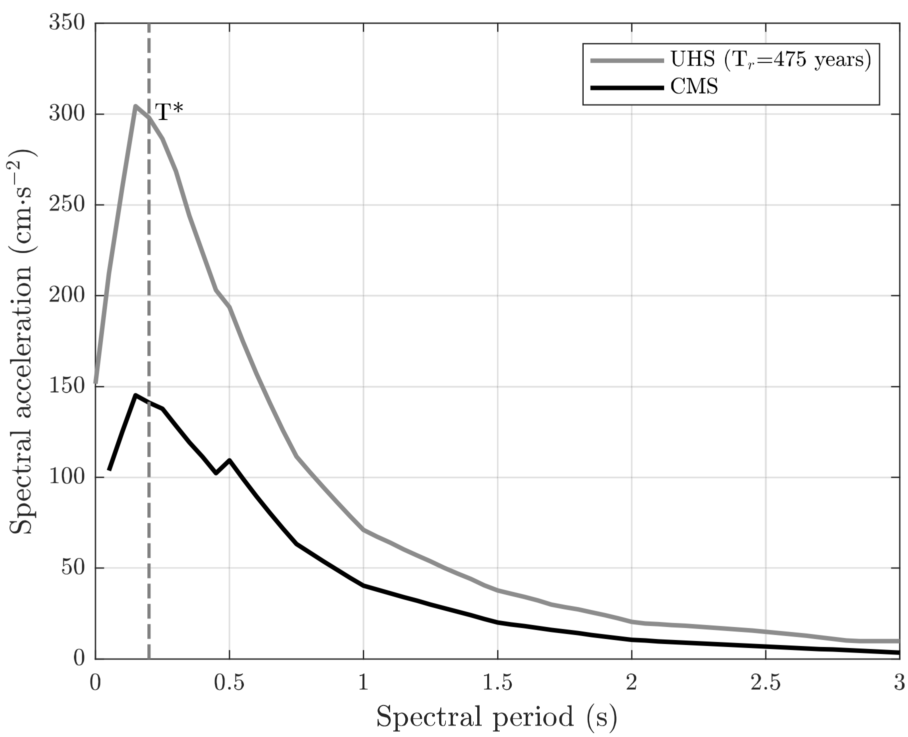

Fig. 12. Conditional Mean Spectrum and Uniform Hazard Spectrum at the reference site with T_r=475 years. Sa(0.2 s)=297.9 cm·s^{-2}, T^*=0.2 s, mean(R,M,ε)= 4.63 M_w, 8.40 km, 6.9.

Different types of lunar habitats have been proposed in the literature, including inflatable, 3D-printed and underground constructions (Ruess et al., 2006). A structure with a fundamental vibration period equal to T^*=0.2 s (same used for the CMS example in Fig. 12) may correspond to a typical lunar habitat. For a seismic response analysis of this hypothetical structure, either one could use the UHS or the CMS spectrum depicted in Fig. 12. Also, a mean response spectrum can be used, like those shown in Fig. 5, but must be evaluated at the m and r of interest for a specific period range (Baker, 2011).

The target spectrum selection to be used in a seismic analysis will depend on different factors, including the structure characteristics, the seismicity of the studied region and the probability level associated with the target $\mathrm{Sa}(T^*)$ (Baker, 2011). Another critical factor to consider for this selection is the value of ε, since it determines the shape of the CMS. For instance, the case presented in Fig. 12, ε takes a positive value in the CMS, producing lower amplitudes than the UHS spectrum. Negative ε values may occur for other hazard environments or a different T^*, resulting in a CMS spectrum greater than the UHS (Baker, 2007).

4. Conclusions

A calculation of the Moon's seismic hazard at the Taurus-Littrow Valley is performed using the PSHA methodology. This work highlights the importance of characterizing the expected ground accelerations on the Moon's surface caused by shallow seismic activity through hazard curves, deaggregation scenarios and response spectra (UHS and CMS). These results show that probable seismic activity of the Lee-Lincoln lobate scarp represents a potential hazard to future structures in the selected study zone. Thus, similar lobate scarps near to future settlement locations should be identified and characterized to evaluate their implications on the seismic performance of the envisioned structures and ensure their resilience and safety.

The presented results are preliminary since the limited available data prevent a better understanding of the lunar seismic nature. In this aspect, one of the significant limitations is the absence of GMPEs that realistically represents the lunar environment. The development of these models was considered beyond the scope of this work and is identified as future research, which can be done once better quality seismic data are recorded in a longer time window. Therefore, it is recommended that future missions in the upcoming lunar explorations focus on collecting reliable seismic and geologic data (Haviland et al., 2021) to reduce uncertainties and refine the hazard models. Collecting more data using modern sensors will allow for the development of Moon-only GMPE and seismic fault models that consider the unique characteristics of the lunar seismic environment, such as the absence of liquid water in the ground, heterogeneity of the lunar crust, and the long duration of moonquakes.

Acknowledgments

We thank L. Ospina, I.C. Gómez and L.V. Prado for their suggestions in the selection of the GMPEs and the study site characterization. We also thank the LROC team for enabling the use of lunar data with the LROC QuickMap application. The authors would like to acknowledge the financial support for the presented work provided by a research grant from the Universidad del Valle (Colombia), as part of the project "Methodology for characterization of the seismic hazard, generation of synthetic accelerograms and design spectra for the Moon" (C.I 21078). This work was supported in part by a Space Technology Research Institutes Grant #80NSSC19K1076 from NASA's Space Technology Research Grants Program.

References

Abrahamson NA, Silva WJ, Kamai R. Summary of the ASK14 ground motion relation for active crustal regions. Earthquake Spectra 2014;30(3):1025–55. doi:10.1193/070913EQS198M.

Aki M. Maximum likelihood estimate of b in the formula logN = a-bM and its confidence limits. Bulletin of the Earthquake Research Institute, University of Tokyo 1965;43(2):237–9.

Akkar S, Bommer JJ. Empirical equations for the prediction of PGA, PGV, and spectral accelerations in Europe, the mediterranean region, and the Middle East. Seismological Research Letters 2010;81(2):195–206. doi:10.1785/gssrl.81.2.195.

Atkinson GM, Boore DM. Modifications to existing ground-motion prediction equations in light of new data. Bulletin of the Seismological Society of America 2011;101(3):1121–35. doi:10.1785/0120100270.

Baker JW. Measuring bias in structural response caused by ground motion scaling. Pacific Conference on Earthquake Engineering 2007;(056):1–6. doi:10.1002/eqe.

Baker JW. Conditional mean spectrum: Tool for ground-motion selection. Journal of Structural Engineering 2011;137(3):322–31. doi:10.1061/(ASCE)ST.1943-541X.0000215.

Baker JW. Introduction to probabilistic seismic hazard analysis. White Paper Version 2013;2.0.1:79.

Banks ME, Watters TR, Robinson MS, Tornabene LL, Tran T, Ojha L, Williams NR. Morphometric analysis of small-scale lobate scarps on the Moon using data from the Lunar Reconnaissance Orbiter. Journal of Geophysical Research E: Planets 2012;117(3):1–11. doi:10.1029/2011JE003907.

Benaroya H. Reliability of structures for the Moon. Structural Safety 1994;15(1-2):67–84. doi:10.1016/0167-4730(94)90053-1.

Benaroya H. Building habitats on the Moon: engineering approaches to lunar settlements. Springer Praxis Books. Springer, 2018.

Bommer JJ. Deterministic vs. probabilistic seismic hazard assessment: An exaggerated and obstructive dichotomy. Journal of Earthquake Engineering 2002;6(sup001):43–73. doi:10.1080/13632460209350432.

Bommer JJ, Scherbaum F, Bungum H, Cotton F, Sabetta F, Abrahamson NA. On the use of logic trees for ground-motion prediction equations in seismic-hazard analysis. Bulletin of the Seismological Society of America 2005;95(2):377–89. doi:10.1785/0120040073.

Bommer JJ, Stafford PJ, Alarcón JE, Akkar S. The influence of magnitude range on empirical ground-motion prediction. Bulletin of the Seismological Society of America 2007;97(6):2152–70. doi:10.1785/0120070081.

Burke JD. Taurus-Littrow Valley. 2018. URL: https://www.britannica.com/print/article/1076595; accessed: 2021-07-20.

Bussey DB, McGovern JA, Spudis PD, Neish CD, Noda H, Ishihara Y, Sorensen SA. Illumination conditions of the South Pole of the Moon derived using Kaguya topography. Icarus 2010;208(2):558–64. doi:10.1016/j.icarus.2010.03.028.

Cohen BA, Team MI. Geohazards on the Moon and the importance of the international lunar network. In: Annual Meeting of the Lunar Exploration Analysis Group. 2009. p. 20.

Duennebier F, Sutton GH. Thermal moonquakes. Journal of Geophysical Research 1974;79(29):4351–63. doi:10.1029/jb079i029p04351.

Dunbar B. Moon's South Pole in NASA's landing sites. 2019. URL: https://www.nasa.gov/feature/moon-s-south-pole-in-nasa-s-landing-sites; accessed: 2021-06-20.

Frohlich C, Nakamura Y. Possible extra-Solar-System cause for certain lunar seismic events. Icarus 2006;185(1):21–8. doi:10.1016/j.icarus.2006.07.002.

Goins NR, Dainty AM, Toksöz MN. Seismic energy release of the Moon. Journal of Geophysical Research 1981;86(B1):378. doi:10.1029/jb086ib01p00378.

Gupta ID. The state of the art in seismic hazard analysis. ISET Journal of Earthquake Technology 2002;39(428):311–46.

Gutenberg B, Richter C. Frequency of earthquakes in California. Bulletin of the Seismological Society of America 1944;34:185–8.

Hanks TC, Kanamori H. A moment magnitude scale. Journal of Geophysical Research: Solid Earth 1979;84(B5):2348–50. doi:10.1029/JB084iB05p02348.

Hargitai H, Kereszturi A. Encyclopedia of planetary landforms. Springer-Verlag New York, 2015.

Haviland HF, Weber RC, Neal CR, Lognonné P, Raphaël F, Schmerr N, Nagihara S, Grimm R, Currie DG, Agnello D, Watters TR, Panning MP, Johnson CL. The lunar geophysical network landing sites science rationale. The Planetary Science 2021;doi:10.48550/arXiv.2107.06451.

Kawamura T, Lognonné P, Nishikawa Y, Tanaka S. Evaluation of deep moonquake source parameters: Implication for fault characteristics and thermal state. Journal of Geophysical Research: Planets 2017;122(7):1487–504. doi:10.1002/2016JE005147.

Khan A, Mosegaard K. An inquiry into the lunar interior: A nonlinear inversion of the Apollo lunar seismic data. Journal of Geophysical Research E: Planets 2002;107(6). doi:10.1029/2001je001658.

Kramer SL. Geotechnical earthquake engineering. Prentice-Hall International Series in Civil Engineering and Engineering Mechanics, 1996.

Kumar PS, Sruthi U, Krishna N, Lakshmi KJP, Menon R, Amitabh , Gopala Krishna B, Kring DA, Head JW, Goswami JN, Kiran Kumar AS. Recent shallow moonquake and impact-triggered boulder falls on the Moon: New insights from the Schradinger basin. Journal of Geophysical Research: Planets 2016;121(2):147–79. doi:10.1002/2015JE004850.

Latham G, Ewing M, Dorman J, Lammlein D, Press F, Toksoz N, Sutton G, Duennebier F, Nakamura Y. Moonquakes. Science 1971;174(4010):687–92. doi:10.1126/science.174.4010.687.

Lognonné P, Johnson C. Planetary seismology. Treatise on Geophysics 2007;volume 10,(Chatper 3):69–122.

Maghareh A, Gomez D, Dyke SJ, Bobet A, Ramirez J, Melosh HJ, Modiriasari A, Theinat AK. Resilience for permanent extraterrestrial habitats. In: Lunar and Planetary Science Conference. volume 49th; 2018. p. 1–6.

Mohanty R, Kumar PS, Raghukanth ST, Lakshmi KJ. The long-lived and recent seismicity at the lunar orientale basin: Evidence from morphology and formation ages of boulder avalanches, tectonics, and seismic ground motion. Journal of Geophysical Research: Planets 2020;125(12). doi:10.1029/2020JE006553.

Mottaghi S, Benaroya H. Design of a lunar surface structure. II: Seismic structural analysis. Journal of Aerospace Engineering 2015;28(1):04014053. doi:10.1061/(asce)as.1943-5525.0000396.

Nakamura Y. Shallow moonquakes: How they compare with earthquakes. In: Lunar and Planetary Science Conference. volume 11; 1980. p. 1847–53.

Nakamura Y. Farside deep moonquakes and deep interior of the Moon. Journal of Geophysical Research E: Planets 2005;110(1):1–12. doi:10.1029/2004JE002332.

Nakamura Y, Dorman J, Duennebier F, Ewinga M, Lammlein D, Latham G. High-frequency lunar teleseimic events. In: 5th Lunar Conference. volume 3; 1974. p. 2883–90.

Nakamura Y, Latham GV, Dorman HJ. Apollo Lunar Seismic Experiment—Final summary. Journal of Geophysical Research 1982;87(S01):A117. doi:10.1029/jb087is01p0a117.

Nakamura Y, Latham GV, Dorman HJ, Ibrahim ABK, Koyama J, Horvath P. Shallow moonquakes: Depth, distribution and implications as to the present state of the lunar interior. In: Lunar and Planetary Science Conference. volume 10; 1979. p. 2299–309.

NASA . NASA's Lunar exploration program overview. 2020. URL: www.nasa.gov/specials/artemis/.

Nunn C, Garcia RF, Nakamura Y, Marusiak AG, Kawamura T, Sun D, Margerin L, Weber R, Drilleau M, Wieczorek MA, Khan A, Rivoldini A, Lognonné P, Zhu P. Lunar seismology: A data and instrumentation review. Space Science Reviews 2020;216(5). doi:10.1007/s11214-020-00709-3.

Oberst J. Unusually high stress drops associated with shallow moonquakes. Journal of Geophysical Research 1987;92:1397–405. doi:10.1029/JB092iB02p01397.

Oberst J, Nakamura Y. A seismic risk for a lunar base. In: The Second Conference on Lunar Bases and Space Activities of the 21st Century. volume 1; 1992. p. 231–3.

Reid RL. Space place. Civil Engineering Magazine Archive 2020;(1):64–73. doi:10.1061/ciegag.0001450.

Ruess F, Schaenzlin J, Benaroya H. Structural design of a lunar habitat. Journal of Aerospace Engineering 2006;19(3):133–57. doi:10.1061/(asce)0893-1321(2006)19:3(133).

Schleicher L, Schmerr N, Watters T, Banks M, Bensi M. Constructing a preliminary probabilistic seismic hazard analysis for the moon. In: Lunar Planetary Science Conference, 2020 Abstract. volume 3064; 2020. .

Schmelzbach C, Stähler S, Schmerr N, Knapmeyer M, Sollberger D, Edme P, Khan A, Brinkman N, Ferraioli L, Robertsson J, Giardini D. Exploring the near-surface at the lunar south pole with geophysical tools 2020;doi:10.48550/arXiv.2009.12807.

Schmitt HH, Petro NE, Wells RA, Robinson MS, Weiss BP, Mercer CM. Revisiting the field geology of Taurus–Littrow. Icarus 2017;298:2–33. doi:10.1016/j.icarus.2016.11.042.

Shi Y, Bolt BA. The standard error of the magnitude-frequency b value. Bulletin of the Seismological Society of America 1982;72(5):1677–87. doi:10.1785/BSSA0720051677.

Sianko I, Ozdemir Z, Khoshkholghi S, Garcia R, Hajirasouliha I, Yazgan U, Pilakoutas K. A practical probabilistic earthquake hazard analysis tool: case study Marmara region. Bulletin of Earthquake Engineering 2020;18(6):2523–55. doi:10.1007/s10518-020-00793-4.

Sollberger D, Schmelzbach C, Robertsson JOA, Greenhalgh SA, Nakamura Y, Khan A. The shallow elastic structure of the lunar crust: New insights from seismic wavefield gradient analysis. Geophysical Research Letters 2016;43(19):10078–87. doi:10.1002/2016GL070883.

Taylor GJ. Future scientific exploration of Taurus-Littrow. In: Ryder G, Schmitt HH, Spudis PD, editors. Geology of the Apollo 17 Landing Site. 1992. p. 57.

Theinat AK, Modiriasari A, Bobet A, Melosh HJ, Dyke SJ, Ramirez J, Maghareh A, Gomez D. Lunar lava tubes: Morphology to structural stability. Icarus 2020;338. doi:10.1016/j.icarus.2019.113442.

Wang JP, Lin YH. Application of bayesian calculation to determine logic-tree weights for ground motion prediction equations: Seismological case studies in Taiwan. Engineering Geology 2021;294(August):106347. doi:10.1016/j.enggeo.2021.106347.

Watters TR, Weber RC, Collins GC, Howley IJ, Schmerr NC, Johnson CL. Shallow seismic activity and young thrust faults on the Moon. Nature Geoscience 2019;12(6):411–7. doi:10.1038/s41561-019-0362-2.

Wells D, Coppersmith K. New empirical relationships among magnitude, rupture length, rupture width, rupture area, and surface displacement. Bulletin of the Seismological Society of America 1994;84:974–1002.

Wiemer S, Wyss M. Minimum magnitude of completeness in earthquake catalogs: Examples from Alaska , the Western United States, and Japan. Bulletin of the

Seismological Society of America 2000;90(August):859–69. doi:10.1785/0119990114.

Williams NR, Watters TR, Pritchard ME, Banks ME, Bell JF. Fault dislocation modeled structure of lobate scarps from Lunar Reconnaissance Orbiter Camera digital terrain models. Journal of Geophysical Research E: Planets 2013;118(2):224–33. doi:10.1002/jgre.20051.

Zalachoris G, Rathje EM. Ground motion model for small-to-moderate earthquakes in Texas, Oklahoma, and Kansas. Earthquake Spectra 2019;55(1):1–20. doi:10.1193/022618EQS047M.

Appendix A. Ground Prediction Equations

I Bommer-07

- *Equation:*
  $\log_{10}(\mathrm{PSA}(T)) =$
  $b_1 + b_2 M_\mathrm{w} + b_3 M_\mathrm{w}^2 + (b_4 + b_5 M_\mathrm{w}) \log_{10}\sqrt{R_{jb}^2 + b_6^2} + f(S, F)$
- *Parameters:*
  R_{jb} = Joyner–Boore distance.
  $b_1, b_2, b_3, b_4, b_5, b_6$ = Regression coefficients.
  $f(S, F)$ = Site and faulting style function.
- *Applicability:*
  Magnitude: 3.0-7.6 M_w.
  Distance: <100 km.
  Spectral period: 0-0.5 s.

II Akkar-10

- *Equation:*
  $\log(\mathrm{PSA}(T)) =$
  $b_1 + b_2 M + b_3 M^2 + (b_4 + b_5 M) \log\sqrt{R_{jb}^2 + b_6^2} +$
  $b_7 S_S + b_8 S_A + b_9 F_N + b_{10} F_R + \varepsilon\sigma$

- *Parameters:*
  R_{jb} = Joyner–Boore distance.
  M = Moment magnitude.
  $b_1, b_2, b_3, b_4, b_5, b_6, b_7, b_8, b_9, b_{10}$ = Regression coefficients.
  F_N, F_R = Flag variables for style of faulting.
  S_S, S_A = Flag variables for soil type.
  ε = Number of standard deviations above or below the mean value of log(PSA).
  σ = Standard deviation.

- *Applicability:*
  Magnitude: 5-7.6 M_w
  Distance (R_{rup}): <100 km
  Spectral period: 0-3.0 s

III **AB-11**

- *Equation:*
  $Y' = YF$
  $\log_{10} F =$
  $\max(0, 3.89 - 0.67\mathbf{M}) - \max(0, 2.93 - 0.51\mathbf{M}) \log(R_{\text{jb}} + 10)$
  Y is the predicted amplitude shown below:
  $\ln Y = F_M(\mathbf{M}) + F_D(R_{jb}, \mathbf{M}) + F_S(V_{S30}, R_{JB}, \mathbf{M}) + \varepsilon\sigma_T$
- *Parameters:*
  M = Moment magnitude.
  Y = Ground motion intensity (PSA).
  R_{jb} = Joyner–Boore distance.
  F_M = Magnitude scaling function.
  F_D = Distance function.
  F_S = Site amplification function.
  ε = Number of standard deviations above or below the mean value of log(PSA).
  σ = Standard deviation.
- *Applicability:*
  Magnitude: 5-8 M_w.
  Distance (R_{jb}): <200 km.

Spectral period: 0-10 s.

IV **ZR-19**

- *Equation:*

  $IM = F \cdot IM_{HA15}$

  $\ln F = C_{adj} + F_M + F_R + F_S$

  IM_{HA15} is the ground motion defined as:

  $\log IM_{HA15} = c_0 + c_1 M + c_2 M^2 + c_3 \log R$

- *Parameters:*

  IM = Ground motion intensity (PSA).
  C_{adj} = Adjustment factor as a function of the structural period.
  F_M = Magnitude scaling factor.
  F_R = Distance scaling factor.
  F_S = Site effects scaling factor.
  M = Moment magnitude.
  c_0, c_1, c_2, c_3= Regression coefficients.
  R= Effective point-source distance.

- *Applicability:*

  Magnitude: 3.0-5.8 M_w.
  Distance (hypocentral): <500 km.
  Spectral period:0-10 s.

V **ASK-14**

- *Equation:*

  $\ln PSA(g) =$

  $f_1 + F_{RV} f_7 + F_N f_8 + F_{AS} f_{11} + f_5 + F_{HW} f_4 + f_6 +$

  $f_{10} + \text{Regional}(V_{s30}, R_{\text{rup}})$

- *Scaling functions:*

  $f_1\left(M, R_{\text{rup}}\right)$, $f_4(R_{jb}, R_{\text{rup}}, R_x, R_{y0}, W, \text{dip}, Z_{TOR}, M)$,

  $f_5(\widehat{Sa}_{1180}, V_{s30})$, $f_6(Z_{\text{TOR}})$, $f_7(M)$, $f_8(M)$,

  $f_{10}(Z_{1.0}, V_{s30})$, $f_{11}(CR_{jb})$.

- *Parameters:*

  M = Moment magnitude.
  CR_{jb} = Centroid R_{jb}.
  R_{jb}= Joyner-Boore distance.
  R_{rup}= Rupture distance.
  R_x= Horizontal distance from top edge of rupture.
  R_{y0}= Horizontal distance from the end of the rupture measured parallel to strike.
  Z_{TOR}= Depth to top of rupture.
  F_{RV}= Flag for reverse faulting.
  F_N = Flag for normal faulting.
  F_{AS}= Flag for aftershocks.
  V_{s30}= Shear-wave velocity over the top 30 m.
  Z_1= Depth to Vs=1.0 km·s^{-1} at the site.
  $\widehat{Sa}_{1180}$= Median PGA for Vs30=1180 m·s^{-1}.
  F_{HW}=Flag for hanging wall sites.
  Dip = Fault dip in degrees.
  W = Down-dip rupture width (km).

- *Applicability:*

  Magnitude: 3.0-8.5 M_w.
  Distance (R_{rup}): 0-300 km.
  Spectral period:0-10 s.